URSI GASS 2020, Rome, Italy, 29 August - 5 September 2020

Embedded Element Patterns in Hierarchical Calibration of Large Distributed Arrays

Stefan J. Wijnholds
ASTRON, Dwingeloo, The Netherlands

Abstract

PM

1 Introduction

Large radio astronomical aperture array systems usually have a hierarchical design in which the receiving elements are grouped in subarrays, often referred to as stations, which together operate as an interferometer array. Examples of such systems are the Low Frequency Array (LOFAR) [1] and the low-frequency component of the Square Kilometre Array (SKA-LOW) [2]. Such systems require calibration at different aggregation levels to ensure high-quality scientific data products: station level calibration is required to form station beams with sufficient quality and stability and array level calibration is required to meet the performance criteria for the interferometer array [3].

Antenna measurements using drones and developments in computational electromagnetics allow us to make validated predictions of the embedded element patterns of the individual antennas in such large arrays [4]. In this paper, I discuss how this knowledge may support station-level and array-level calibration and what accuracy is required to do so. In this discuss, I pay particular attention to the question whether this accuracy can be achieved by using only a single average embedded element pattern (EEP) for all antennas or whether modelling of individual EEPs is required in the context of LOFAR and SKA-LOW.

2 Station level calibration

The aim of station calibration is to keep track of electronic drift in the individual receive paths in the station due to, e.g., temperature variations and aging of electronic components. This information is required to form a well-defined beam in the desired direction. Simulations have shown that the impact of ignoring EEP difference in the modelling of the intra-station visibilities causes a systematic error in the station calibration solutions that varies with sidereal time [5]. If these calibration solutions would be fed back to the beamforming system, the station beam would exhibit a drift-like effect even when the station electronics would be perfectly stable. I will refer to this as *calibration drift*. As the aim of station calibration is to improve system performance, calibration drift should be less than electronic drift, at least when direct feedback of station calibration solutions to the beamforming system is being considered. The combination electronic drift and calibration drift gives rise to decorrelation in the station beamformer and to drift of the station beam(s) formed. Below, I provide derivations that can be used to set requirements such that these detrimental effects remain within acceptable limits.

The excitation of the individual elements of the array in response to a plane wave impinging on the array at a given frequency can be represented by a phasor, whose phase described the geometrical delay of the wave across the array w.r.t. a common reference point. If the beamformer works perfectly, all these phasors are aligned parallel before addition thereby maximising the amplitude of the resultant vector in the complex plane. Based on this argument, it is easily seen that a RMS phase error σ_φ will result in a vector that is only a fraction $\cos(\sigma_\varphi)$ of the length achievable by perfect addition. In the power domain, the beamformer efficiency given RMS phase errors σ_φ is therefore

$$\eta_{\mathrm{BF}} = \cos^2(\sigma_\varphi) \approx 1 - \sigma_\varphi^2, \tag{1}$$

where the approximation proposed by John Ruze [6], holds if σ_φ is expressed in radians. This implies that a beamformer efficiency of 99% requires $\sigma_\varphi \leq 5.7^\circ$ while a beamformer efficiency of 98% requires $\sigma_\varphi \leq 8.1^\circ$.

Although Eq. (1) is insightful, it does not set a limit on the inter-element amplitude variations. For this, we need to consider the output SNR of the beamformer,

$$\mathrm{SNR}_{\mathrm{BF}} = \frac{\mathbf{w}^H \mathbf{R}_\mathrm{s} \mathbf{w}}{\mathbf{w}^H \mathbf{R}_\mathrm{n} \mathbf{w}}, \tag{2}$$

where $\mathbf{w}$ is the vector with beamformer weights and $\mathbf{R_s}$ and $\mathbf{R_n}$ are the array covariance matrices for the signal and noise respectively [7]. Assuming a source of unit power in the phase center ($\mathbf{R}_\mathrm{s} = \mathbf{1}\mathbf{1}^H$, where $\mathbf{1}$ denotes a vector filled with ones) and elements with unit noise power ($\mathbf{R} = \mathbf{I}$, where $\mathbf{I}$ denotes the identity matrix), Eq. (2) simplifies to

$$\mathrm{SNR}_{\mathrm{BF}} = \frac{\mathbf{w}^H \mathbf{1}\mathbf{1}^H \mathbf{w}}{\mathbf{w}^H \mathbf{I} \mathbf{w}} = \frac{\left|\mathbf{w}^H \mathbf{1}\right|^2}{\mathbf{w}^H \mathbf{w}}. \tag{3}$$

This equation can be used to compare the output SNR of the beamformer for various error distributions against the

output SNR of an error-free beamformer. As an example, I will assume beamformer weights with zero-mean Gaussian noise with standard deviation ε, $\mathcal{N}(0,\varepsilon)$, on its real and imaginary parts, i.e., $w_p = 1+\mathcal{N}_p(0,\varepsilon)+\mathrm{j}\mathcal{N}_p(0,\varepsilon)$, where p denotes the element index. This gives

$$\mathrm{SNR}_{\mathrm{BF}} = \frac{\left|\sum_p 1+\mathcal{N}_p(0,\varepsilon)-\mathrm{j}\mathcal{N}_p(0,\varepsilon)\right|^2}{\sum_p 1+2\mathcal{N}_p(0,\varepsilon)+2\left|\mathcal{N}_p(0,\varepsilon)\right|^2}. \quad (4)$$

Since the errors are assumed to have zero mean, the linear error terms will cancel if the number of elements in the array, P, is sufficiently large. In the same limit, the quadratic term in the denominator will converge to $2P\varepsilon^2$. Taking into account that the ideal beamformer would have an SNR of P, the beamformer efficiency in this example becomes

$$\eta_{\mathrm{BF}} = \frac{\mathrm{SNR}_{\mathrm{BF}}}{P} = \frac{1}{1+2\varepsilon^2} \approx 1-2\varepsilon^2, \quad (5)$$

where the approximation for small errors is based on the Taylor series of $1/(1+x)$. This result implies that a beamformer efficiency of 99% requires $\varepsilon \leq 7.1\%$ while a beamformer efficiency of 98% requires $\varepsilon \leq 10\%$.

In theory, the station beams can be predicted based on a priori information like station beam weights, operational antennas and their EEPs. In practice, this prediction will not be perfect and array level calibration will have to handle deviations between the actual station beams and the predicted station beams. If this deviation is constant, long calibration intervals can be used in direction-dependent calibration to estimate this deviation very accurately. This task becomes more challenging when this deviation is varying with time. This issue can be analysed by considering the contribution of visibility V_{ij} to the imaging of a source with flux S at some point in the field-of-view towards which the stations involved have gains g_i and g_j when this contribution is integrated over the calibration interval *tau*:

$$V_{ij} = \frac{1}{\tau}\int_{-\tau/2}^{\tau/2} \frac{g_i}{g_{0i}}\frac{\overline{g_j}}{\overline{g_{0j}}} S \mathrm{d}t, \quad (6)$$

where g_{0i} and g_{0j} are the calibration corrections applied.

Initially, the changes in the direction-dependent gains g_i and g_j will, to first order, be linear. Assuming that the calibration routine perfectly estimates the average value of the gains over the calibration interval, we can describe g_i as $g_i = g_{0i}+\alpha_i t$. The visibility is then described by

$$V_{ij} = \frac{1}{\tau}\int_{-\tau/2}^{\tau/2} \frac{g_{0i}+\alpha_i t}{g_{0i}}\frac{\overline{g_{0j}+\alpha_j t}}{\overline{g_{0j}}} S \mathrm{d}t. \quad (7)$$

Performing the integration gives

$$V_{ij} = S + \frac{1}{12}\frac{\alpha_i}{g_{0i}}\frac{\overline{\alpha_j}}{\overline{g_{0j}}}\tau^2 S = S + \Delta S. \quad (8)$$

If the bias due to drift of the station beam is uncorrelated between visibilities, drift effectively acts like another source of noise that we would like to keep below the thermal noise

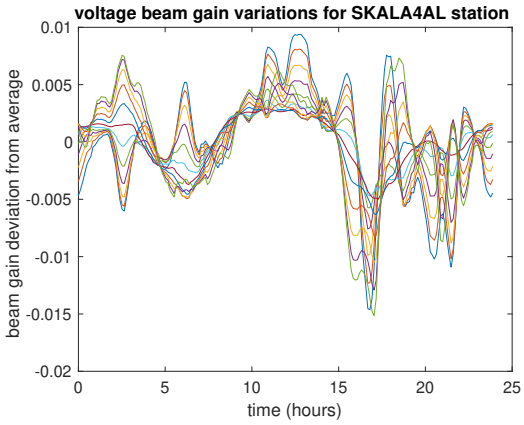

Figure 1. Local relative station beam gain variations along the cross-section through the main beam with largest variability as function of time since 22 August 2018, 0:00:00 UTC.

in the image. Keeping it below 20% of the thermal noise implies that

$$\frac{|\Delta S|}{S} \leq \frac{1}{5}\frac{\mathrm{SEFD}/\sqrt{B\tau}}{S} = \frac{1}{5}\frac{1}{\mathrm{SNR}}, \quad (9)$$

where SEFD refers to the Source Equivalent Flux Density of the system and SNR is the SNR of the source with flux S used for direction-dependent calibration.

Assuming that the drift rates follow a random distribution with RMS magnitude α and the true gains are nominally identical with magnitude g_0, Eq. (9) can be written as

$$\frac{1}{12}\frac{\alpha^2}{g_0^2}\tau^2 \leq \frac{1}{5}\frac{1}{\mathrm{SNR}}, \quad (10)$$

which implies a limit on the rate of change of the relative error on the directional response of the stations of

$$\frac{\alpha}{g_0} \leq \sqrt{\frac{12}{5}}\frac{1}{\sqrt{\mathrm{SNR}}}\frac{1}{\tau} = \sqrt{\frac{12}{5}}\sqrt{\frac{\mathrm{SEFD}}{S\sqrt{B\tau}}}\frac{1}{\tau}. \quad (11)$$

Calibration intervals are usually chosen such that the SNR towards the (clusters of) calibration sources is at least 5 to 10. To find a conservative estimate, I will assume an SNR of 10. In LOFAR, common solution intervals for calibration of direction-dependent instrumental effects are 5 to 10 minutes. To find a conservative estimate, I will assume 10 minutes, i.e., $\tau = 600$ s. These values give $\alpha/g_0 \leq 0.082$ %/s. For SKA-LOW, the allowed rate of change will be higher owing to its higher sensitivity. The lower SEFD implies that a shorter integration time is sufficient to perform direction-dependent calibration with the same density of directions and SNR. This relaxes the requirement, i.e., direction-dependent calibration is able to keep up with faster changing station beams.

The impact of ignoring EEP differences between antennas was assessed in simulation for a SKA-LOW station consisting of SKALA4AL antennas located at the AAVS site

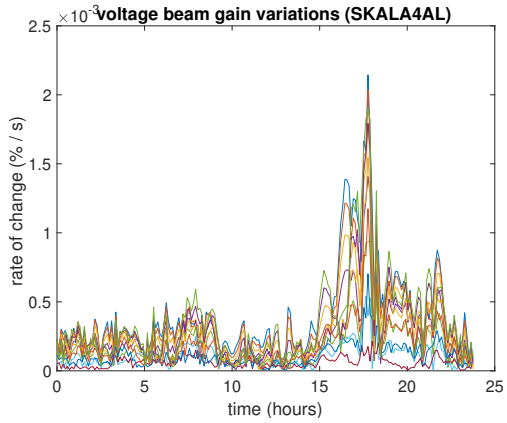

Figure 2. Rate of change of the local relative station beam gain variations sow in Fig. 1.

(-27.6° S, 116.7° E). Mock visibility data were created at 110 MHz based on the Haslam map [8] and EEPs from an EM-simulation validated by drone measurements [9]. For calibration, model visibilities were created based on the Haslam map assuming an identical EEP for all elements equal to te average EEP from the EM-simulation. Calibration was performed for 200 instances in time spread over 24 hours starting at 22 August 2018 at 0:00:00 UTC. The estimated gains were applied to classical delay beamformer weights to calculate a station beam for each of the 200 instances. Fig. 1 shows the local relative station beam gain variations for a number of points sampling the cross-cut through the station main beam where the highest variability was found. By taking the difference between the station beam gain predictions for consecutive time instances, an estimate was calculated for the rate of change of the relative error. The result is shown in Fig. 2.

These results indicate that, although ignoring EEP differences in station calibration results in a bias, the rate of change of this bias is slow enough that continuous re-calibration of.a station during an observation will not results in station beam variations at a rate of change that direction-dependent calibration at array level will not be able to deal with. Also, even at the most unfavourable instance in time, the RMS phase variation induced by this bias on the gain solutions for the individual receive paths within a station is expected to be less than 4°. This only causes 0.5% decorrelation in the station beamformer, which is well within the allowed budget for beamforming errors. We may thus conclude that a priori knowledge of an average EEP is sufficient for station calibration. In both simulation and experiments with LOFAR and the AAVS prototype station, we found, however, that errors in the currently used source model may cause an even larger bias than ignoring EEP variations. This needs to be validated carefully before opting for continuous re-calibration of the station during an observation.

3 Array level calibration

Direction-dependent calibration is a pre-requisite for high-dynamic range imaging [10]. LOFAR Epoch-of-Reionization observations and, to a lesser extend, LOFAR survey observations therefore perform direction dependent calibration in $\sim$10 to even $\sim$ 100 directions [11, 12]. Direction-dependent calibration in LOFAR does not only provide ionospheric corrections, but corrections for discrepancies between the station beam model and the actual station beam. As the station beam shape is mainly determined by the array factor, an inaccurate model of the EEPs of the antennas within a station is usually not a major issue if direction-dependent calibration is applied.

The EEPs play a far more important role in flux calibration. For flux calibration, the telescope is pointed at a flux calibrator to establish the telescope gain shortly before or after the observation of the target field [12]. Unfortunately, the telescope gain of an aperture array varies significantly with pointing direction, mainly due to the (average) EEP and projection effects. As a result, the telescope gain towards the flux calibrator and towards the target field, which may be separated by $\sim$100° on the sky, may differ considerably and this needs to be taken into account during flux calibration transfer from the calibrator to the target field. This issue has been discussed extensively in the LOFAR project as plans are being made towards its upgrade to LOFAR 2.0. Considering that the absolute flux scale at 150 MHz is about 5% uncertain (Reinout van Weeren, private communication). To ensure that flux calibration transfer does not add significantly to this, the System Requirements for LOFAR 2.0 now specify that *"LOFAR 2.0 shall provide a flux calibration of sources with a reproducibility of less than 2% independent of the sky position above an elevation fo 10 degrees."*

To meet this reproducibility target, we need to know the overall gain of the station in a given direction, i.e., the sum of all individual EEPs after phasing up towards the direction of interest, across the sky within 1.4% assuming that the errors towards the calibrator and towards the target field are unrelated and may therefore be added quadratically. Since calculation of the isolated element pattern (IEP) is much less computationally demanding than calculation fo the average EEP (aEEP), the difference between the IEP and the aEEP was studied in detail for the LOFAR LBA system [13]. The results indicate that for the relatively sparse LBA outer configuration of the Dutch LOFAR stations, the differences between the IEP and aEEP remain within the 1.4% limit for boresight angles up to 60° at fiducial frequencies of 32, 44, 57 and 70 MHz. For the more densely packed LBA inner array, the situation is more complicated. At 32 MHz, the requirement is met for boresight angles up to 60°. At 44, 57 and 70 MHz, however, the requirement is only met over a more restricted range of boresight angles, about 30°, 40° and 25° at 44, 57 and 70 MHz respectively. Therefore, a full EM simulation of an entire LOFAR station may

thus be required to achieve the desired flux calibration reproducibility.

A similar analysis was done for an SKA-LOW station [14]. At 50 MHz, the difference between the IEP and the aEEP reach levels of 40% within 45° from boresight. This warrants a full EM simulation. At 110 and 350 MHz, the other two frequencies assessed in [14], the agreement between the IEP and aEEP is much better across the boresight angle range considered (up to 45°). However, the results still show a number of boresight angle where a similar requirement as for LOFAR would only be marginally satisfied with differences at the 3% level. It thus seems necessary to calculate the aEEP for the SKA-LOW stations to achieve the desired level of flux calibration reproducibility.

4 Conclusions

In this paper, I assessed the need for accurate modelling of individual EEPs in large, distributed aperture arrays like LOFAR and SKA-LOW. Although using an average EEP in station calibration causes a bias in the calibration solutions, this effect in itself does not seem to pose unacceptable degradation of system performance. However, station calibration should not worsen system performance (for this reason, LOFAR uses fixed station calibration tables for significant periods (few months) of time) and one should ensure that the combination of EEP modelling errors and source modelling errors together still gives acceptable results. For flux calibration transfer, knowledge of the average EEP is sufficient, but the average EEP cannot be replaced by the isolated element pattern as that would give rise to unacceptably poor flux calibration reproducibility in many scenarios.

5 Acknowledgements

The author would like to thank Mark Waterson, Daniel Hayden, Maria Grazia Labate and Robert Laing for the in-depth discussion on the practical impact of station calibration and Reinoud van Weeren for raising the importance knowing the gain of the full array across the sky for flux calibration transfer from one field to another.

References

[1] M. P. van Haarlem *et al.*, "LOFAR: The Low Frequency Array," *Astronomy & Astrophysics*, vol. 556, no. A2, pp. 1–53, Aug. 2013.

[2] P. E. Dewdney, P. J. Hall, R. T. Schilizzi, and T. J. L. W. Lazio, "The Square Kilometre Array," *Proceedings of the IEEE*, vol. 97, no. 8, pp. 1482–1496, Aug. 2009.

[3] S. J. Wijnholds, S. van der Tol, R. Nijboer, and A. J. van der Veen, "Calibration challenges for future radio telescopes," *IEEE Signal Processing Magazine*, vol. 27, no. 1, pp. 30–42, Jan. 2010.

[4] G. Virone *et al.*, "Strong Mutual Coupling Effects on LOFAR: Modeling and In-Situ Validation," *IEEE Transactions on Antennas and Propagation*, vol. 66, no. 5, pp. 2581–2588, May 2018.

[5] S. J. Wijnholds, M. Arts, P. Bolli, P. Di Ninni, and G. Virone, "Using Embedded Element Patterns to Improve Aperture Array Calibration," in *International Conference on Electromagnetics in Advanced Applications*, Granada, Spain, 9 – 13 Sep. 2019.

[6] J. Ruze, "Antenna tolerance theory - A review," *Proceedings of the IEEE*, vol. 54, no. 4, pp. 633–640, Apr. 1966.

[7] B. D. Jeffs *et al.*, "Signal Processing for Phased Array Feeds in Radio Astronomical Telescopes," *IEEE Journal of Selected Topics in Signal Processing*, vol. 2, no. 5, pp. 635–646, Oct. 2008.

[8] C. Haslam, C. Salter, H. Stoffel, and W. Wilson, "A 408 MHz all-sky continuum survey II - The atlas of contour maps," *Astronomy & Astrophysics Supplement Series*, vol. 47, pp. 1–2, 4–51, 53–142, Jan. 1982.

[9] G. Virone, F. Paonessa, L. Ciorba, and B. P., "Results on UAV measurements," in *SKA-LOW Station Calibration Task meeting*, Florence, Italy, 1 – 3Jul. 2019.

[10] K. Iheanetu *et al.*, "Primary beam effects in radio astronomy antennas - I. Modelling of the Karl G. Jansky Very Large Array (VLA) L-band beam using holography," *Monthly Notices of the Royal Astronomical Society*, vol. 485, no. 3, pp. 4107–4121, May 2019.

[11] S. Yatawatta *et al.*, "Initial deep LOFAR observations of the epoch of reionization windows – I. The north celestial pole," *Astronomy & Astrophysics*, vol. 550, no. A136, pp. 1–17, 2013.

[12] T. W. Shimwell *et al.*, "The LOFAR Two-metre Sky Survey - I. Survey description and preliminary data release," *Astronomy & Astrophysics*, vol. 598, no. A104, pp. 1–22, Feb. 2017.

[13] P. Di Ninni *et al.*, "Electromagnetic analysis and experimental validation of the LOFAR radiation patterns," *International Journal of Antennas and Propagation*, vol. 2019, no. 9191580, pp. 1–12, Jan. 2019.

[14] P. Di Ninni, M. Bercigli, P. Bolli, G. Virone, and W. S. J., "Mutual Coupling Analysis for a SKA1-LOW Station," in *European Conference on Antennas and Propagation (EuCAP)*, Krakow, Poland, 31 Mar. – 5 Apr. 2019.